Mansoura Engineering Journal

Volume 33 | Issue 1 Article 3

12-1-2020

Control Scheme for a Grid Connected Permanent Magnet Synchronous Generator Driven Wind Turbine.

Mohamed El-Sayed Mohamed
Associate Professor., IEEE. Member Electrical Engineering Department., Mansoura University., Mansoura., Egypt., mrashed@mans.edu.eg

Control Scheme for a Grid Connected Permanent Magnet Synchronous Generator Driven Wind Turbine

منظومة للتحكم فى مولد تزامنى دائم التغذية مرتبط بالشبكة و يدار بتربينة رياح

Mohamed Rashed; *IEEE. Member*
Electrical Engineering Department, Mansoura University, Egypt
e-mail: mrashed@mans.edu.eg

ملخص: يقدم البحث نظام مقترح للتحكم فى مولد تزامنى دائم التغذية مرتبط بالشبكة ويدار بتربينة رياح. يهدف نظام التحكم المقترح إلى تعقب القدرة القصوى المتولدة من تربينة الرياح وضمان تشغيل المولد التزامنى بكفاءة عالية بدون إستخدام حساسات لسرعة الرياح أو لسرعة المولد التزامنى .وعليه فانه تم إقتراح خوارزم رياضى مبتكر وبسيط يعتمد على النموذج الرياضى للمولد التزامنى وفيه يتم حساب كلا من سرعة وموضع وقيمة الفيض القاطع للعضو الدوار للمولد التزامنى .وبالإضافة لما سبق فإنه تم تصميم خوارزم رياضى لإضعاف المجال القاطع للعضو الدوار يضمن تشغيل المولد عند حدود الجهد والتيار الأقصى ويتيح زيادة مدى التشغيل للمولد عند سرعات الرياح العالية والتى تكون عندها القدرة المتاحة من تربينة الرياح أعلى من القدرة القصوى للمولد .تم أيضا دراسة تأثيرنسبة الخطأ فى ثوابت النموذج الرياضى للمولد والمستخدمة فى خوارزمات التحكم والحساب على دقة النظام المقترح فى تعقب القدرة القصوى لتربينة الرياح .تم عمل النمذجة التفصيلية والمحاكاة للنظام المقترح باستخدام حزمة برامج جاهزة وتم اختبار أداء النظام المقترح عند ظروف تشغيل مختلفة وكان أداء النظام مستقرا وعاليا.

Abstract: Direct coupling of Wind Turbine WT becomes feasible with modern Permanent Magnet Synchronous Generators PMSG. This paper presents a sensorless Maximum Power Point Tracker MPPT for a grid connected PMSG direct driven fixed pitch WT. The MPPT objectives are: to track the maximum output power form the WT and to guarantee efficient operation of PMSG. A new and simple rotor position, speed and rotor flux magnitude estimator based on the PMSG model is proposed. The estimator evades using the stator current derivatives calculation, which is an inherent drawback of the back-EMF based estimators. The PMSG estimated speed is fed to the MPPT to calculate the reference stator currents. A field weakening algorithm is also designed to widen the operating speed range of the PMSG. The sensitivity of the proposed sensorless MPPT to PMSG parameters mismatch is investigated and studied. Finally, the control scheme is tested and investigated under various operating conditions and demonstrated excellent steady state and dynamic performance.

Keywords: MPPT, sensorless, PMSG, wind turbine

I. INTRODUCTION

Due to concerns about environmental consequences of using fossil fuel and the steep price rises of the oil, worldwide power generation particularly from wind energy has received great attention. The advances in power electronics and digital control offer sensorless variable speed operation of WT Generators WTG and thus opportunity of tracking maximum output under varying wind conditions. Doubly Fed Induction Generators DFIG driven WT are widely used as variable speed wind energy conversion system. The main advantage is reduced power ratings of the used power electronics, i.e. 25% of the nominal power of the DFIG. However, DFIG operates at relatively high speed and thus requires bulky and costly gearboxes as speed increaser. In contrast, direct drive of low speed and high torque generators offers reduction of overall size, lower cost and quick response to wind fluctuations. Meanwhile, the advances in the permanent magnet materials increased the viability of the PMSG for direct-drive application, [1]. Nevertheless, efficient operation of the PMSG requires accurate information about the rotor position. Nowadays, sensorless speed and position estimation schemes for PMSG are reliable and accurate especially when operating at relatively high speeds. Back-EMF based rotor position estimation methods are widely used, in which the back-EMF vector is detected and thus information about rotor position is extracted, [2]. However, back-EMF based techniques are suffering from increased system noise, which originates from the calculation of the current derivatives, [3]. In the literature, many maximum power tracking algorithms for WT are presented. These can be classified into two main categories: 1) WT model-based algorithms, 2) maximum power point searching algorithms. In model based algorithms, the optimal WT speed is determined using the WT model and the measured wind speed, [4]. On the other hand, maximum power point searching algorithms use the hill climbing techniques to track the maximum power operating point, [5]-[7]. Such schemes do not require any information about the WTG system. However they are computationally intensive, slow convergent and sensitive to system noise. In [5], a sensorless maximum power extraction algorithm based on hill-climb searching method has been developed. Wherein, an intelligent memory is trained on-line to identify the maximum power trajectory line. Also, in [2] a variable speed IPMSG is presented where the rotor speed is estimated based on back-EMF detection. Maximum output power from the generator is attained by tracking the

Accepted March 31, 2008

maximum output power from the WT and minimizing the generator losses.

Many WTG control schemes use diode rectifier after the PMSG, [6], [8]-[9]. In [6], a PMSG driven WT followed by a diode bridge is used to charge a battery controlled by a DC-DC converter. A maximum power point searching technique has been proposed where the output power of the WT is measured and the duty cycle of the DC-DC converter is adjusted based on the difference between two successive output powers. In [8] a DC-DC chopper is used to control the diode rectifier output voltage and hence the PMSG speed to follow the value of the optimal reference speed. Moreover, in [9], a PMSG with diode rectifier supplying the generated power to a load via a Current Controlled Inverter CCI is proposed. The CCI is controlled to adjust the dc link voltage to track the maximum output power from the PMSG. Actually, the use of diode rectifiers provides cost effective interface of the PMSG, however the high power/volume ratio and the control flexibility of the PMSG are compromised since the PMSG stator currents are square waveforms of 120° and the power flow is unidirectional. In contrast, extracting sinusoidal currents from the PMSG increases its power density and efficiency, [10].

In this paper a grid connected direct drive sensorless PMSG driven fixed pitch WT is proposed. Wherein, a sensorless maximum power tracker is designed and a new and simple rotor position, speed and rotor flux magnitude estimator is proposed. The PMSG is connected to the grid via a three phase back-to-back PWM converters. The PMSG side converter is controlled to extract maximum output power from the WT and to maintain operation of the PMSG at optimal torque/current ratio. Field weakening control algorithm is designed for operation at speeds above the base speed. The objectives are: to limit the stator current and voltage magnitude to their permissible values and to extract as much power as possible from the WT. Furthermore, the sensitivity of the proposed sensorless MPPT to the PMSG parameters mismatch is investigated and studied.

The paper is organized into five sections. The system modeling and description are given in section II. In section III, the proposed sensorless MPPT is detailed and discussed. Simulation results are given and studied in section IV. Finally, conclusions are drawn and given in section V.

II. System Modelling and Description

Fig. 1 shows the block diagram of the proposed sensorless control scheme for a PMSG driven WT. The system comprises of direct driven PMSG, fixed pitch WT and two interfacing converters. The PMSG phase currents are measured and transformed from the stationary abc reference frame to xy rotating reference frame. The x-axis stator current component i_{sx} is the reactive power current component while i_{sy} is the active power current component. The measured currents i_{sx} and i_{sy} are compared to the reference values and the errors are fed to high bandwidth PI controllers. The outputs of the PI controllers are the reference stator voltage components $u_{sx\text{-}ref}$ and $u_{sy\text{-}ref}$. It should be noted that the converter is operating at relatively high modulation index and thus the voltage drop due dead time and other inverter nonlinearities is negligible in comparison to the converter's output voltage. Therefore, the input-output transfer function of the converter is considered equal to unity and thus the applied stator voltage vector to the PMSG is assumed equal to the reference stator voltage vector. On the other hand, the grid side converter is used to control the DC link voltage and the reactive power injected to the grid.

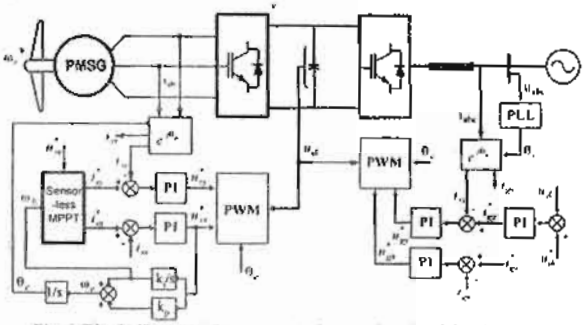

Fig. 1 Block diagram of the proposed sensorless PMSG driven WT

A. PMSG Modeling

The PMSG iron losses are neglected and the mechanical losses are represented by a simple friction model. Thus, the model of the PMSG driven WT formulated in synchronous rotating reference frame xy that rotates at angular speed of ω_e is given as (see Fig. 2.b), [3]:

$$\dot{\bar{i}}_s = -(a_1 I + J\omega_e)\bar{i}_s - Ja_2\omega_r\bar{\psi}_r + a_2\bar{u}_s \qquad (1\text{-a})$$

$$\dot{\bar{\psi}}_r = -J(\omega_e - \omega_r)\bar{\psi}_r \qquad (1\text{-b})$$

$$\dot{\omega}_r = \frac{1}{H}\left(T_e - B\omega_r - T_l\right) \qquad (1\text{-c})$$

where: $\omega_r = \dot{\theta}_r$; $\omega_e = \dot{\theta}_e$; $T_e = 1.5P\left(\psi_{rx} i_{sy} - \psi_{ry} i_{sx}\right)$

$\bar{u}_s = [u_{sx}\ u_{sy}]^T$; $\bar{i}_s = [i_{sx}\ i_{sy}]^T$; $\bar{\psi}_r = [\psi_{rx}\ \psi_{ry}]^T$;

$\psi_r = \sqrt{\psi_{rx}^2 + \psi_{ry}^2}$; $\psi_{rx} = \psi_r \cos(\theta_r - \theta_e)$;

$\psi_{ry} = \psi_r \sin(\theta_r - \theta_e)$; $a_1 = R_s/L_s$; $a_2 = 1/L_s$;

$$J = \begin{bmatrix} 0 & -1 \\ 1 & 0 \end{bmatrix};\quad I = \begin{bmatrix} 1 & 0 \\ 0 & 1 \end{bmatrix};$$

subscripts s and r denote stator and rotor variables respectively. x, y indicate direct and quadrature axis respectively. u and i refer to voltage and current respectively. ψ_r the magnitude of the rotor flux linkage. ω_r is the rotor speed in rad/s. θ_r, $\hat{\theta}_r$ and θ_e are the rotor position, the estimated rotor position and the synchronous rotating reference frame position respectively, (see Fig. 2.b). R_s is the stator winding resistance. L_s is the stator winding self inductance. H and B are the lumped inertia and friction constants of the WTG system respectively. T_T is the WT output torque. T_e is the PMSG developed torque. The

equivalent circuit and the phasor diagram shown in Fig. 2 abbreviate the PMSG model given in (1).

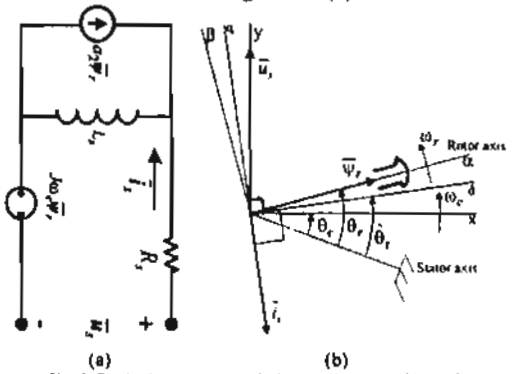

(a) (b)

Fig. 2 Equivalent circuit and phasor diagram of PMSG

It should be noted that in Fig. 2.b, four reference frames are introduced. These are: the stator reference frame, (stationary reference frame); the synchronous rotating reference frame, xy; the estimated rotor flux reference frame, dq and the rotor reference frame, αβ.

B. Wind Turbine Modeling

The WT blades convert fraction of the wind energy to mechanical power. The WT energy conversion efficiency depends on the design parameters of the turbine blades, the wind speed and the WT speed. The steady-state delivered mechanical power by the WT P_t is given by, [11]:

$$P_t = 0.5\rho A_r C_p(\lambda,\beta) w^3 \quad (2\text{-a})$$

$$\lambda = \omega_r R_r / w \quad (2\text{-b})$$

$$C_p(\lambda,\beta) = c_1\left(\frac{c_2}{\lambda_i} - c_3\beta - c_4\beta^x - c_5\right)e^{-(c_6/\lambda_i)} \quad (2\text{-c})$$

$$\frac{1}{\lambda_i} = \frac{1}{(\lambda + 0.02\beta)} - \frac{0.003}{(\beta^3 + 1)} \quad (2\text{-d})$$

where: C_p is the power coefficient, (efficiency). β is the pitch angle, degree. λ is the tip speed ratio. w is the wind speed, m/s. ω_r is the WT rotor speed, rad/s. R_r is the WT rotor-plane radius, m. ρ is the air density, kg/m^3. A_r is the area swept by the WT rotor, m^2. c_1, c_2, c_3, c_4, c_5, c_6 and x are WT model parameters. The parameters of the WT used in the present paper are given in Appendix, Table 1.

The WT characteristics are calculated from (2) using the parameters given in Appendix, Table 1. Fig. 3.a illustrates the variation of the C_p with the tip speed ratio and the pitch angle. It should be noted that, pitching the WT blades out of the wind direction reduces the efficiency of the WT. Also, for particular pitch angle, the WT maximum efficiency C_{pmax} occurs at specific tip speed ratio, which is called the optimal tip speed ratio λ_{op}. This reveals that maximising the output power from the WT can be achieved by adjusting the WT speed in proportion to the wind speed keeping the tip speed ratio equal to λ_{op}. Fig. 3.b illustrates the calculated WT power-speed characteristics at different wind speeds.

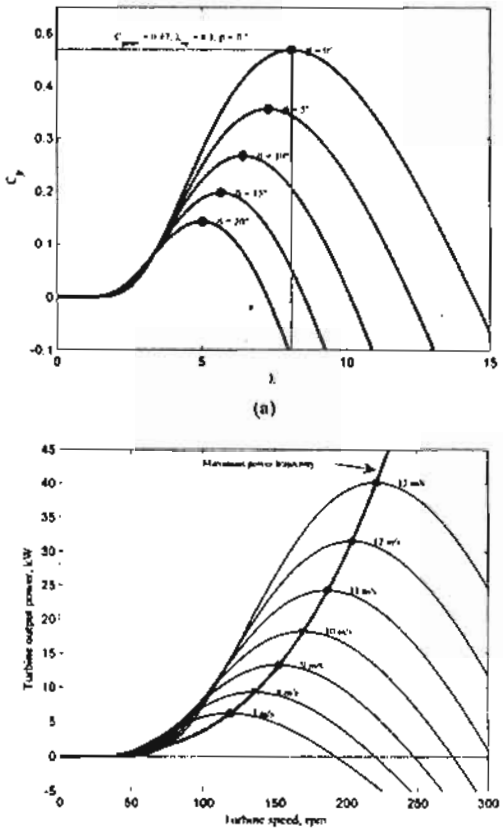

(a) (b)

Fig. 3 WT characteristics a) C_p characteristics b) power-speed characteristics

By substituting (2.b) into (2.a), the WT power can be rewritten as:

$$P_t = -\frac{\rho A_r R^3}{2}\frac{C_p(\lambda,\beta)}{\lambda^3}\omega_r^3 \quad (3)$$

It is noticeable from (3) that the output power from the WT is maximum and proportional to the cubic of the turbine speed if the tip speed ratio is maintained equal to λ_{op} and hence C_p is equal to C_{pmax}. Therefore, from (3), the maximum WT output power is:

$$P_{t-max} = -k_t\omega_r^3 \quad (4)$$

where $k_t = \frac{\rho A_r R^3}{2}\frac{C_{pmax}}{\lambda_{op}^3}$

Equation (4) characterizes the maximum power trajectory line that is shown in Fig. 3.b. In conclusion, maximum output power from the WT is guaranteed if the PMSG is controlled to satisfy (4).

C. Grid side Converter Modeling

The grid side converter is connected to the grid via a series filter (inductor) as shown in Fig. 1. The grid voltages and currents are sensed and used as feedback to the converter controller. A PLL is used to track the position of the grid

voltage vector, θ_v, [12]. The model of the grid side converter in a general rotating reference frame that rotates at angular speed of ω_g is given by:

$$\dot{i}_g = -(a_3 I + J\omega_g)\bar{i}_g + a_4(\bar{u}_g - \bar{u}_{conv}) \; ; \; \dot{\theta}_v = \omega_g \quad (5)$$

Where: $a_3 = R_f / L_f$ and $a_4 = 1/L_f$; subscript g denotes grid variables. R_f and L_f are the series filter resistance and inductance respectively. $\bar{u}_g$ and $\bar{u}_{conv}$ are the grid and the converter voltage space vectors respectively. ω_g is the estimated angular speed of the grid voltage vector.

III. PMSG Sensorless Control Scheme

In the proposed sensorless control scheme of the PMSG, u_{sx-ref} is directly fed to a PI controller to estimate the speed of the synchronous rotating reference frame, xy. The output of the PI controller is ω_e while the output of the PI controller integrator is ω_E, see Fig. 1. The position of the rotating reference frame θ_e is determined by direct integration of ω_e. The model of the proposed estimator is thus given by:

$$\omega_e = -k_p u_{sx-ref} + \omega_E \; ; \; \dot{\omega}_E = -k_i u_{sx-ref} \; ; \; \dot{\theta}_e = \omega_e \quad (6)$$

It should be noted that, at steady state $\omega_e = \omega_E = \omega_r$ although there is steady state position difference between θ_e and θ_r. Moreover, $u_{sx-ref} = 0$. This is clearly demonstrated by the phasor diagram shown in Fig. 2.b. Furthermore, because of the slow dynamics of the power tracking process, ω_e is considered equal to the estimated rotor speed of the PMSG.

In the following subsections, the proposed sensorless MPPT, the sensitivity of the MPPT to parameters mismatch and the rotor flux estimator will be studied.

A. Sensorless MPPT

The aims of the proposed MPPT are: to track the maximum output power from the WT and to operate the PMSG at the optimal torque/current ratio. The first aim is realized via satisfying (4) while the second aim is achieved by retaining the stator current vector perpendicular to the PMSG rotor axis (i.e. $i_{sd} = 0$) and thus minimizing the PMSG stator losses. The input to the MPPT block is the estimated PMSG speed and u_{sy-ref}. Owing to ω_E is the output of an integrator (see Fig. 1) and thus free of ripples, it is proposed to use ω_E as the input to the MPPT block instead of ω_e. This is to reduce the level of ripples propagated through the control system loops. The PMSG steady state model, the WT maximum power trajectory (4), u_{sy-ref} and the estimated speed ω_E are processed by the MPPT to determine the PMSG estimated rotor position $\hat{\theta}_r$, the estimated rotor flux magnitude $\hat{\psi}_r$ and the optimal values of $i_{sxy-ref}$ maintaining $i_{sd} = 0$. However, at high wind speeds, operation at maximum power points of the WT is no longer possible since the WT developed torque and speed are higher than the corresponding PMSG nominal values. Noticeably, from Fig. 3.b that the possible approach to sustain the system in operation at high wind speeds is to operate the PMSG-WT away from the maximum power trajectory line and towards higher speed operating points. For this purpose, field weakening strategy is designed and employed to operate the WTG at higher speeds and to retain the stator current and voltage of the PMSG at their permissible limits and to develop as high torque as possible. To this extent, the operation of the proposed MPPT algorithm is divided into two modes. Mode-1is designated for operation at speeds below the base speed while Mode-2 is devoted for operation at speeds above the base speed.

Mode-1

In mode-1 i_{sd} is set equal to zero. Thus, the steady state model of the PMSG in the estimated rotor reference frame dq can be reduced to the following:

$$u_{sd} = -\hat{L}_s \omega_E i_{sq} \; ; \; u_{sq} = \hat{R}_s i_{sq} + \omega_E \hat{\psi}_r \; ; \quad (7\text{-a})$$

$$T_e = 1.5 P \hat{\psi}_r i_{sq} \; ; \; u_s = \sqrt{u_{sd}^2 + u_{sq}^2} \quad (7\text{-b})$$

where ^ denotes to estimated parameters, (i.e. parameters used in the control algorithm).

From (7) and Fig. 2.b, the estimated rotor position is given by:

$$\hat{\theta}_r = \theta_e + \tan^{-1}(u_{sd}/u_{sq}) \quad (8)$$

From (7) and (4) i_{sq} is calculated as follows:

$$i_{sq} = \frac{2}{3P^2\hat{\psi}_r}(\hat{B}\omega_E - \hat{k}_t \omega_E^2 / P) \quad (9)$$

Then, the reference stator currents i_{sx-ref} and i_{sy-ref} are calculated as follows, (see Fig. 2.b):

$$i_{sx-ref} = i_{sd}\cos(\hat{\theta}_r - \theta_e) - i_{sq}\sin(\hat{\theta}_r - \theta_e) \quad (10\text{-a})$$

$$i_{sy-ref} = i_{sd}\sin(\hat{\theta}_r - \theta_e) + i_{sq}\cos(\hat{\theta}_r - \theta_e) \quad (10\text{-b})$$

Mode-2

In mode-2, field weakening strategy is applied where i_{sd} and i_{sq} are calculated to retain the applied stator voltage and current at their nominal values. Once more, from the steady state model of the PMSG and by neglecting the stator resistance voltage drop i_{sd} and i_{sq} are calculated as follows:

$$i_{sd} = \frac{U_{s-nom}^2 - \hat{L}_s^2\omega_E^2 I_{s-nom}^2 - \hat{\psi}_r^2\omega_E^2}{2\hat{L}_s\omega_E^2\hat{\psi}_r} \quad (11\text{-a})$$

$$i_{sq} = \sqrt{I_{s-nom}^2 - i_{sd}^2} \; ; \quad (11\text{-b})$$

and

$$u_{sd} = \hat{R}_s i_{sd} - \hat{L}_s \omega_E i_{sq} \quad (12\text{-a})$$

$$u_{sq} = \hat{R}_s i_{sq} + \hat{L}_s \omega_E i_{sd} + \omega_E \hat{\psi}_r \; ; \; u_s = \sqrt{u_{sd}^2 + u_{sq}^2} \quad (12\text{-b})$$

where: U_{s-nom}, I_{s-nom} are the nominal values of the stator voltage and current vector magnitudes respectively.

Then, $\hat{\theta}_r$ and i_{sxy_ref} are calculated from (6) and (8) respectively. The switching between mode-1 and mode-2 is performed based on the value of i_{sd} that is calculated from (11-a). Mode-1 is activated if i_{sd} has positive value otherwise mode-2 is activated.

B. Sensitivity to Parameters Mismatch

This section is devoted to study the sensitivity of the proposed sensorless MPPT to PMSG parameters mismatch. Typically, the stator resistance and the rotor flux are varying due to temperature rise. R_s increases by a value up to 50%

of its nominal value, however the rotor magnet flux decreases by a value down to -20% of its nominal value, [3]. To study, the effect of Rs and rotor flux mismatch on the sensorless MPPT, the steady state model of PMSG-WT and the speed estimator model given by (6) are used to calculate the WT output power and the operating speed for wide range of wind speeds and different degree of parameters mismatch. Numerical solution has been adopted since the model of the PMSG-WT system is highly nonlinear. The difference between the calculated output power from the WT and the maximum available power is calculated. Also, the deviation in the operating speed from the optimal value is determined. The numerical (iterative) calculation algorithm is implemented in Matlab code. First; calculations have been performed for 100% stator resistance mismatch while the rotor flux is retained equal to its nominal value. The deviation in the operating speed and in the WT output power from the maximum power operating point is recorded at different wind speeds. The results are shown in Fig. 4. It is noted that the proposed sensorless MPPT scheme is insensitive to stator resistance mismatch.

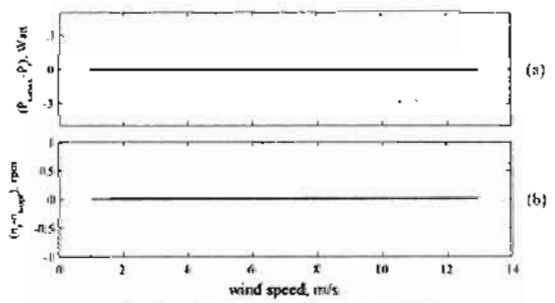

Fig. 4 Sensitivity to R_s mismatch, (100%)

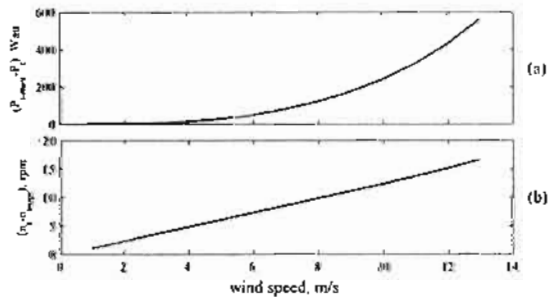

Fig. 5 Sensitivity to rotor flux mismatch, (-20%)

The calculations have also been performed but for a -20% mismatch in the rotor flux. The results are shown in Fig 5. It is noticeable from Fig. 5 that the divergence of the operating point away from the maximum power operating point is significant. This reveals that the proposed MPPT is sensitive to rotor flux mismatch. For this reason, rotor flux magnitude estimator is proposed to update the value of the rotor flux. The design of the proposed estimator will be studied in the next section.

C. Rotor Flux Magnitude Estimator

A simple rotor flux estimator is designed to update the value of the rotor flux magnitude. It should be noted that at steady state the calculated stator voltage magnitude u_s in the MPPT by (7-b) or (12-b) should be exactly equal to the $u_{sy\text{-}ref}$ if the value of the rotor flux magnitude $\hat{\psi}_r$ used is accurate. On the other hand, if there is rotor flux mismatch, there will be difference between the calculated u_s and $u_{sy\text{-}ref}$. Even though, the derivatives of the stator current exist during transient periods, it is neglected since the dynamics of the overall WTG is slow. Therefore, the difference between u_s and $u_{sy\text{-}ref}$ is directly used to estimate the rotor flux magnitude using a simple integral sliding mode controller, see Fig. 6. The estimated rotor flux magnitude is thus given by:

$$\dot{\hat{\psi}}_r = \psi_{r\text{-}nom} + k_f \int \mathrm{sgn}(u_{sy\text{-}ref} - u_s)dt \qquad (13)$$

where: sgn denotes to sign. $\psi_{r\text{-}nom}$ is the rotor flux linkage nominal value.

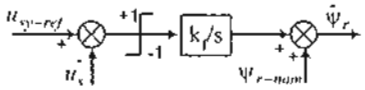

Fig. 6 Rotor flux estimator

The proposed rotor flux estimator is implemented inside the MPPT and the value of estimated rotor flux magnitude $\hat{\psi}_r$ is used in (7)-(12).

IV. Results and Discussion

The proposed sensorless control scheme for PMSG driven WT shown in Fig. 1 and discussed in sections II-III is modeled and simulated in the Matlab environment particularly using the power system simulator, SimPowerSystems and the Simulink toolboxes. The parameters of the PMSG, the WT and the converters used in the simulation are given in Appendix, Table I. IGBT/Diode universal bridge inverter provided by SimPowerSystems toolbox is used in modeling the PMSG and the grid side converters. Sinusoidal type PWM strategy is implemented to synthesis the converters output voltages based on the measured DC link voltage u_{dc} and the converters' reference voltages. The steady state and transient performance of the proposed control scheme are investigated. Also, the tracking performance of the proposed rotor flux estimator is examined.

A. Sudden change in wind speed test

The reference values of the grid side converter are set to: u^*_{dc} = 800 V, i^*_{gx} = 0 A. The wind speed is initially set to 7 m/s. At t = 0.15 s the wind speed is increased to 12 m/s and then returned back to its original value at t = 0.25 s. The results are shown in Fig. 7, 8 and 9. Fig 7.a shows the WT output power (dashed) and the PMSG output power (solid). Fig. 7.b shows ω_r (dashed), ω_E (solid) and ω_e (dotted). ω_e is shifted down just for the purpose of discrimination between the lines. Fig. 7.e illustrates $(\theta_r\text{-}\theta_e)$ (dashed) and $(\theta_r\text{-}\hat{\theta}_r)$ (solid). It is noticeable from Fig. 7.b that the estimated speed is in excellent agreement with the actual PMSG speed. Also, optimal torque/current ratio is sustained. This is evident from the zero values of both $(\theta_r\text{-}\hat{\theta}_r)$ and i_{sa}. Fig. 9 demonstrates the trajectories of the WT output power (dashed) and the PMSG output power (solid) on the WT

power-speed characteristic. The trajectories move from point A (on the 7 m/s power line) to point B (on the 12 m/s power line) and returned back to point A. It is manifest that points A and B lay on the maximum power trajectory line. This reveals that excellent tracking performance of the maximum power point is achieved.

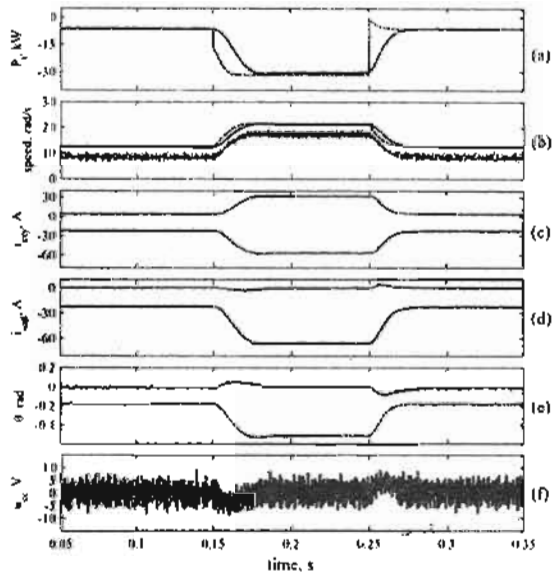

Fig.7 Wind speed change test, PMSG side variables

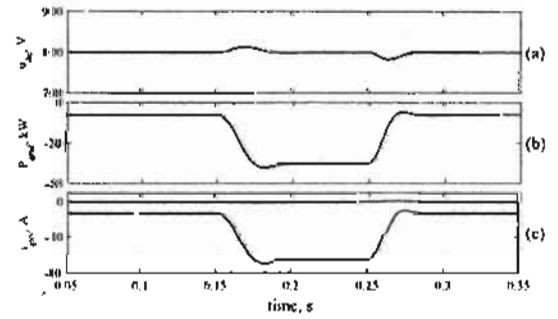

Fig.8 Wind speed change test, grid side converter variables

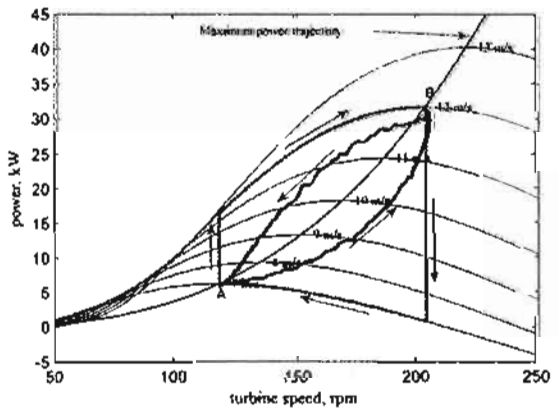

Fig.9 Wind speed Change test, power speed trajectories.

Fig. 8 shows the control variables of the grid side converter. The results show excellent dynamic and steady state performance of grid side converter control scheme.

B. Field weakening operation

Furthermore, the control scheme is tested in the field weakening mode of operation. The wind speed is initially set to 7 m/s. At t = 0.15 s the wind speed is gradually increased by a rate of 15 m/s^2 until it reached a value of 13.5 m/s and then maintained constant until it is suddenly reduced back to 7 m/s, see Fig. 10.e. The magnitude of the stator current and voltage vectors are limited to $I_{s\text{-}nom}$ = 65.5 A, $U_{s\text{-}nom}$ = 360 V respectively. The simulation results are shown in Figs. 10 and 11. It is noted from Fig. 10.d that $i_{s\alpha}$ is equal to zero during the time periods where the wind speed is less the nominal value (12 m/s). At t = 0.5 s, the wind speed achieved its nominal value and the stator voltage and current reached their limit values. After t = 0.5 s, where the wind speed is higher than the nominal value, $i_{s\alpha}$ is increased to deteriorate the rotor flux linkage and thus maintaining the PMSG stator voltage at its limit value, see Fig. 10.e. The WT and the PMSG output powers are shown in Fig. 10.a and their trajectories against the rotor speed are plotted on the WT power-speed characteristics as shown in Fig 11. The trajectories started at point A and moved slowly towards point B and suddenly returned back to point A. It is noted that the traveling of the trajectories was on the maximum power trajectory line until it reached the nominal operating point on the 12 m/s wind speed power curve. Afterward, the field weakening algorithm is activated and managed the trajectories away from the maximum power trajectory line limiting the PMSG stator current and voltage. The obtained results demonstrate stable operation at various operating points including field weakening mode of operation.

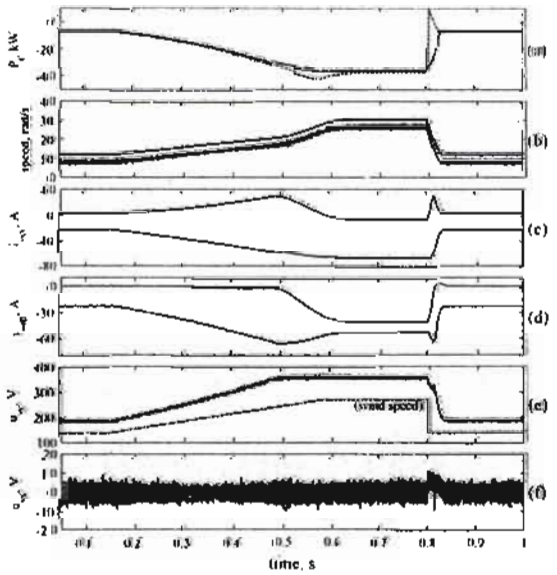

Fig. 10 Field weakening test; PMSG variables

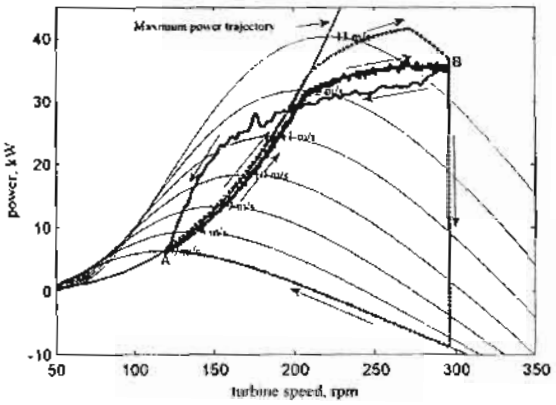

Fig 11 Field weakening test, Power trajectories.

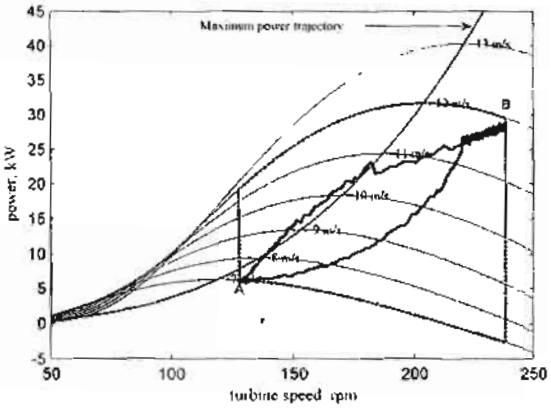

Fig 13 Test results for -20% rotor flux mismatch, power trajectories

C. Parameters Mismatch Test

Moreover, the control scheme sensitivity to rotor flux mismatch is examined. The actual rotor flux magnitude is reduced by 20% of its nominal value. In addition, the rotor flux estimator is switched off while the nominal value of the rotor flux magnitude is used in the control algorithm. The test has been performed under the same operating conditions of the test results shown in Figs. 7-9. The obtained results are shown in Figs. 12 and 13. It is noted from Fig. 13 that operating points A and B deviate from the maximum power trajectory line indicating failure in tracking maximum power point of the WT. Moreover, $i_{sα}$ is not equal to zero that discloses to inefficient operation of the PMSG. The results clearly demonstrate that the proposed control scheme is sensitive to rotor flux magnitude mismatch.

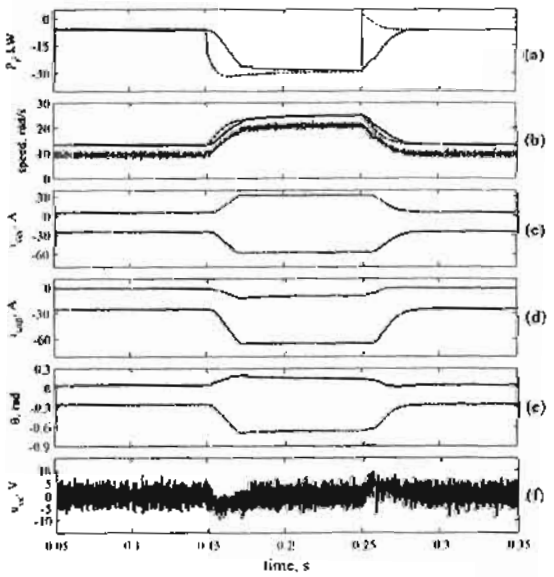

Fig. 12 Test results for -20% rotor flux mismatch; PMSG variables

The sensitivity of the MPPT to stator resistance mismatch is also investigated by simulation. Similar test has been carried out under the same operating conditions of the test results shown in Fig. 12 but with a 100% stator resistance mismatch. The obtained results confirmed the insensitivity of the proposed MPPT to stator resistance mismatch.

D. Rotor Flux Estimator: Tracking Performance test

In this test, the wind speed is set to a constant value of 11 m/s. At t = 0.15 s, the actual rotor flux magnitude is reduced by 20% of its nominal value and returned back to its nominal value at t = 0.25 s. The obtained results are shown in Fig. 14. Fig. 14.f shows the actual (dashed) and the estimated (solid) rotor flux magnitude. It is noticeable that the rotor flux estimator is stable and provides excellent tracking performance. Also, the updating of the rotor flux value maintains the WT operating at the maximum power points, see Fig. 14.a. Moreover, $i_{sα}$ is retained equal to zero providing minimal PMSG stator copper losses.

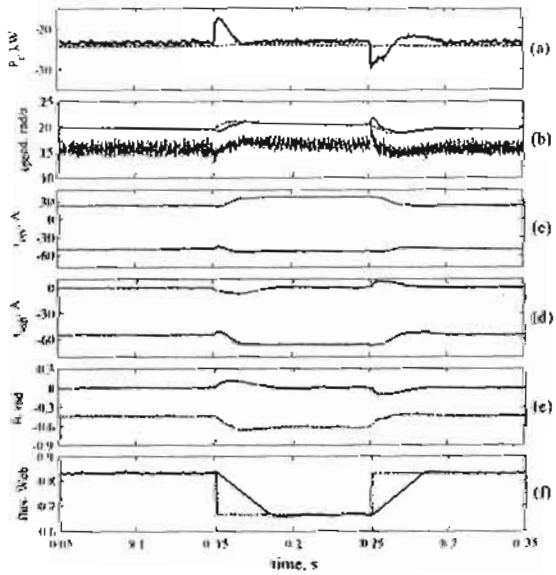

Fig 14 Tracking performance of the rotor flux estimator

V. Conclusions

A new sensorless MPPT for a grid connected PMSG direct driven fixed pitch WT has been proposed and studied. The speed and the position of the rotating reference frame are estimated using the reference stator voltage component u_{sx_ref} and then the rotor position is estimated utilizing the steady state model of the PMSG. In addition, rotor flux magnitude estimator has been proposed. Wherein, the reference stator voltage component u_{sy_ref} is compared with the calculated stator voltage magnitude and the error is used to estimate the rotor flux magnitude. The proposed estimation schemes benefited from avoiding the calculation of the stator current derivatives, which is considered an inherent problem of the well known back-EMF based estimators. At speeds below base speed, the control scheme has been designed to maximize the output power from the WT and to preserve efficient operation of the PMSG. Moreover, field weakening algorithm has been designed to extend the WTG range of operation to wind speeds higher than the nominal value. Sensitivity of the proposed sensorless MPPT to PMSG parameters mismatch has been investigated and studied. The sensorless MPPT has been found insensitive to stator resistance mismatch. Furthermore, the sensitivity of the MPPT to the rotor flux mismatch has been eliminated by employing the proposed rotor flux estimator to update the value of the rotor flux magnitude. The proposed control scheme has been modeled and simulated in the Matlab environment. The simulation results have shown excellent transient and steady state performance under various operating conditions.

VI. References

[1] Zhang J., Cheng M. and Chen Z., "A Novel Stator Interior Permanent Magnet Generator for Direct-Drive Wind Turbines", Proceeding of International Conference on Electrical Machines and Systems, Seoul, Korea, 8-11 October 2007, pp. 723-728

[2] Morimoto S., Nakayama H., Sanada M. and Takeda Y., "Sensorless Output Maximization Control for Variable-Speed Wind Generation System Using IPMSG", IEEE, Transactions On Industry Applications, Vol. 41, No. 1, January/February 2005, pp. 60-67

[3] Rashed M. MacConnell PFA, Stronach AF and Acarnley P. "Sensorless, Indirect-Rotor-Field-Orientation Speed Control of a Permanent Magnet Synchronous Motor with Stator Resistance Estimation", IEEE, Transactions on Industrial Electronics, Vol. 54, No 3, June 2007, pp. 1664-1675.

[4] Senjyu T., Tamaki S., Muhando E., Urasaki N., Kinjo H., Funabashi T, Fujita H and Sekine H., "Wind velocity and rotor position sensorless maximum power point tracking control for wind generation system", Journal of Renewable Energy, Vol. 31, 2006, pp. 1764–1775.

[5] Wang Q. and Chang L., "An Intelligent Maximum Power Extraction Algorithm for Inverter-Based Variable Speed Wind Turbine Systems", IEEE, Transactions on Power Electronics, Vol. 19, No. 5, September 2004, pp. 1242-1249.

[6] Koutroulis E and Kalaitzakis K., "Design of a Maximum Power Tracking System for Wind-Energy-Conversion Applications", IEEE, Transactions on Industrial Electronics, Vol. 53, No. 2, April 2006, pp 486-494

[7] Esmaili R., Xu L., Nichols D. K., "A New Control Method of Permanent Magnet Generator for Maximum Power Tracking in Wind Turbine Application", IEEE, Power Engineering Society General Meeting, Vol. 3, 12-16 June 2005, pp. 2090-2095.

[8] Li W., Abbey C. and Joos G., "Control and performance of Wind Turbine Generators based on Permanent Magnet Synchronous Machines Feeding a Diode Rectifier", 37th IEEE, Power Electronics Specialists Conference, PESC'06, 18-22 June 2006, Pages(s): 1-6

[9] Tan K., and Islam S., "Optimum control strategies in energy conversion of PMSG wind turbine system without mechanical" IEEE, Transactions On Energy Conversion, Vol. 19, No. 2, June 2004, pp 392-399

[10] Lee H.W., Kim T.H. and Ehsani, M., "Practical Control for Improving Power Density and Efficiency of the BLDC Generator", IEEE Transactions on Power Electronics, Vol. 20, No. 1, January 2005, pp. 192-199

[11] Slootweg J.G., De Haan S.W.H., Polinder H., and Kling W.L., "General model for representing variable speed wind turbines in power system dynamics simulations", IEEE, Transactions on Power Systems, vol. 8, No. 1, 2003, pp. 144-151.

[12] Timbus A.V., Teodorescu R., Blaabjerg F., Liserre M. And Rodriguez P., "PLL Algorithm for Power Generation Systems Robust to Grid Voltage Faults", 37th IEEE, Power Electronics Specialists Conference, PESC'06, 18-22 June 2006, Page(s): 1-7

VII. Appendix

Table. I System parameters and controllers gains

WT parameters and specifications	
$c_1 = 0.4$, $c_2 = 199$, $c_3 = 0.58$, $c_4 = 0.002$, $c_5 = 13.2$, $c_6 = 18.4$ and $x = 2.14$	
Nominal wind speed:	12 m/s
Nominal output power:	30 kW
Pitch angle, β:	0°
Blades radius, R:	4.541 m
Air density, ρ:	1.205 kg/m^3
PMSG parameters and ratings	
Nominal L-L voltage:	440 V, 60 Hz
Nominal power:	30 kW
Nominal speed:	200 rpm
Number of pole pairs, (P)	18
Self inductance, L_s:	7 mH
Stator resistance, R_s:	0.13 Ω
Magnet-flux/phase, ψ_{f_rms}:	0.83 web
Lumped friction constant, B:	0.88 Nm.s
Lumped inertia constant, H:	1.6 Nm.s^2
Converters parameters	
Switching frequency:	10 kHz
Dc link voltage, u_{dc}:	800 V
Dc link capacitance	2000 μF
Series filter inductance, L_f:	5 mH
Series filter resistance, R_f:	0.05 Ω
Controllers gains	
PMSG side:	
PI speed estimator gains: $k_1 = 5$, $k_2 = 2500$	
PI current controller gains $k_p = 40$, $k_i = 5000$	
Flux estimator gain: $k_f = 5$	
Grid side:	
PI dc link voltage controller gains: $k_p = 1$, $k_i = 200$	
PI current controller gains: $k_p = 60$, $k_i = 3000$	
PLL PI controller gains: $k_p = 2$, $k_i = 1000$	